

PCCP

Accepted Manuscript



This is an *Accepted Manuscript*, which has been through the Royal Society of Chemistry peer review process and has been accepted for publication.

Accepted Manuscripts are published online shortly after acceptance, before technical editing, formatting and proof reading. Using this free service, authors can make their results available to the community, in citable form, before we publish the edited article. We will replace this *Accepted Manuscript* with the edited and formatted *Advance Article* as soon as it is available.

You can find more information about *Accepted Manuscripts* in the [Information for Authors](#).

Please note that technical editing may introduce minor changes to the text and/or graphics, which may alter content. The journal's standard [Terms & Conditions](#) and the [Ethical guidelines](#) still apply. In no event shall the Royal Society of Chemistry be held responsible for any errors or omissions in this *Accepted Manuscript* or any consequences arising from the use of any information it contains.

Band alignment and charge transfer in rutile-TiO₂/CH₃NH₃PbI_{3-x}Cl_x interfaces

G. A. Nemnes^{a*}, C. Goehry^b, T. L. Mitran^a, Adela Nicolaev^a, L. Ion^a, S. Antohe^a, N. Plugaru^c, A. Manolescu^b

Received Xth XXXXXXXXXXXX 20XX, Accepted Xth XXXXXXXXXXXX 20XX

First published on the web Xth XXXXXXXXXXXX 200X

DOI: 10.1039/b000000x

Hybrid halide perovskite CH₃NH₃PbI_{3-x}Cl_x / rutile-TiO₂ interfaces are investigated by *ab initio* density functional theory calculations. The role of chlorine in achieving enhanced solar cell power conversion efficiencies is in the focus of recent studies, which point to increased carrier mobilities, reduced recombination rates, a driven morphology evolution of the perovskite layer and improved carrier transport across the interface. As it was recently established that chlorine is preferentially localized in the vicinity of the interface and not in the bulk of the perovskite layer, we analyze the changes introduced in the electronic properties by varying the chlorine concentration near the interface. In particular, we discuss the effects introduced in the electronic band structure and show the chlorine role in the enhanced electron injection in the rutile-TiO₂ layer. Taking into account these implications, we discuss the conditions for optimizing the solar cell efficiency in terms of interfacial chlorine concentration.

1 Introduction

Hybrid lead-halide perovskite materials, in particular methylammonium lead halides of formula CH₃NH₃PbX₃ (MAPbX₃) with X = Cl, I, Br, have been in the focus of solar energy research for the past few years as prominent candidates for low-cost high-efficiency solar cells, with power conversion efficiencies (PCEs) steadily rising towards 20%¹⁻³. Two of the key elements identified, which may explain the large PCEs, reside in the unusually large diffusion lengths⁴ and high absorption rate in MAPbX₃ materials. In addition, the methylammonium dipoles may play a significant role in charge separation⁵ and their dynamics has been investigated in a number of studies⁶⁻¹⁰. In spite of the ongoing progress, there are issues of prime importance that need to be resolved, such as the long term stability¹¹ under working conditions and a better understanding of the fundamental aspects related to the charge transfer which govern the device operation, in order to further optimize the power output.

It is well-established that MAPbI_{3-x}Cl_x yields significantly higher efficiencies than the MAPbI₃ counterpart^{12,13} and this behavior has been attributed to several reasons. Primary observations pointed to the enhanced carrier mobilities in MAPbI_{3-x}Cl_x¹⁴, while subsequently the reduced recombination rates were regarded as a more suitable premise¹⁵. The incorporation of chlorine was also investigated in the con-

text of perovskite film growth^{16,17}. Here it was reported that chlorine plays an essential role in the morphology evolution of the perovskite layer, particularly in releasing the excess of the organic compound. Furthermore, X-ray photoelectron spectroscopy investigations revealed that only small amounts of chlorine are found in the perovskite layer, suggesting the remaining chlorine is concentrating near the interface¹⁸. A detailed analysis based on time-resolved photoluminescence, Kelvin-probe force microscopy, transient photovoltage decay and capacitance-voltage measurements has shown that the presence of the chlorine produces an improved carrier transport across the interface rather than in the perovskite crystals¹⁹. Recently, a direct observation of chlorine near the TiO₂/perovskite interface was demonstrated using hard X-ray photoelectron spectroscopy (HAX-PES) at different photon energies and fluorescence yield X-ray absorption spectroscopy (FY-XAS)²⁰.

Motivated by these recent indications for the localization of chlorine near the interface, along with the previous observations of enhanced PCEs, we perform a systematic study of the effects of interfacial chlorine on the band alignment and charge transfer for the TiO₂/MAPbI_{3-x}Cl_x structures. Following the seminal papers of Mosconi et al.²¹ and Colella et al.²², which discuss the role of chlorine at the perovskite/anatase-TiO₂ interface, we investigate by *ab initio* density functional theory (DFT) calculations the perovskite/rutile-TiO₂ interface, focusing on the changes induced by a sequential increase of chlorine concentration. Solar cells based on rutile-TiO₂ have been fabricated²³⁻³⁰ using the transparent oxide either as mesoporous thin films or as nanorod scaffolds, some exhibiting superior performance compared to the anatase counter-

^a University of Bucharest, Faculty of Physics, Materials and Devices for Electronics and Optoelectronics Research Center, P.O. Box MG-11, 077125 Magurele-Ifov, Romania. E-mail: nemnes@solid.fizica.unibuc.ro.

^b School of Science and Engineering, Reykjavik University, Menntavegur 1, IS-101 Reykjavik, Iceland

^c Natl Inst Mat Phys, Magurele 077125, Ifov, Romania

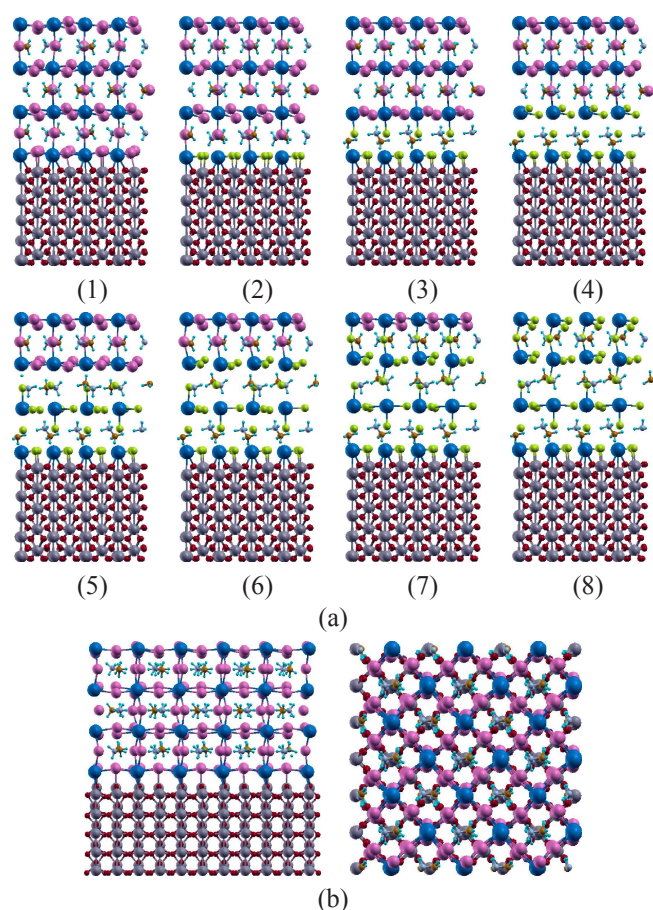


Fig. 1 (a) $\text{TiO}_2/\text{MAPbI}_{3-x}\text{Cl}_x$ slab structures, with increasing concentration of chlorine substituted on iodine. The TiO_2 exposes the (001) surface, on which the (001) perovskite is deposited. The atomic color codes are: Ti (grey), O (red), Pb (blue), I (magenta), Cl (green), while the CH_3NH_3 organic molecules are identifiable within the Pb-I(Cl) cages. For a better description, 2×2 unit cells are represented. (b) Rotated (45°) and top view of the $\text{TiO}_2/\text{MAPbI}_3$ interface.

parts²⁶, using low-temperature solution processing techniques which are adequate for flexible substrate technology. Furthermore, as the electron injection can be influenced by the crystal phase of TiO_2 ²⁵, it is highly important to acquire further knowledge concerning the electronic structure and charge transfer in these types of interfaces.

2 Model structures and Method

The structures under investigation are depicted in Fig. 1, being assembled by TiO_2 -rutile and $\text{MAPbI}_{3-x}\text{Cl}_x$ slabs, oriented perpendicular to the z -direction. Using pre-optimized bulk lattice parameters and atomic coordinates we consider a configuration of minimal stress, which results by coupling the (001)

surface of the perovskite with the (001) TiO_2 -rutile substrate. Each tetragonal perovskite unit cell, with the lattice parameters $a = b = 8.8\text{\AA}$ and $c = 12.5\text{\AA}$, is matched on 2×2 tetragonal TiO_2 -rutile unit cells, of lattice parameters $a = b = 4.5\text{\AA}$ and $c = 2.9\text{\AA}$. In this way, a mismatch of the lattice parameters of the two materials smaller than 3% is achieved. Figure 1(a) shows different systems, with increasing concentration of chlorine substituted on iodine layer by layer, starting with MAPbI_3 until a full replacement has been achieved. The perovskite slabs contain seven alternating layers of Pb-I(Cl) and MA-I(Cl) , while the TiO_2 slab contains five unit cells along the z -direction. The slabs are initially separated by a distance set by the typical bonding lengths of Ti-I and Pb-O . A vacuum distance of 15\AA separates the slabs along the non-periodic z -direction. For clarity, rotated and top views of the $\text{TiO}_2/\text{MAPbI}_3$ interface are shown in Fig. 1(b).

Structural relaxations are performed using the SIESTA package³¹, which provides an appropriate computational framework for relatively large systems. In our calculations we make use of the local density approximation (LDA) in the parametrization of Ceperley and Alder³². The structures were relaxed until the residual forces are less than 0.04 eV/\AA . A double-zeta basis set was employed, constructed by the standard split norm of 0.15 in the split-valence scheme and a value of 100 Ry mesh cut-off was used to set up the real space grid. For the sampling of the Brillouin zone a $3 \times 3 \times 1$ Monkhorst-Pack scheme was employed. Troullier-Martins norm conserving pseudopotentials were used, with their transferability tested in the corresponding bulk structures of the two materials.

Following relaxations, the structures become slightly contracted along the z -direction and, in particular, the outer perovskite layer with chlorine substitutions. This is to be expected as the chlorine based perovskite has a smaller lattice constant compared to the iodine counterpart³³. More specifically, the Ti-Cl bonding length of 2.4\AA is shorter compared to value of 2.8\AA corresponding to Ti-I bonds. The Pb-O bonding lengths are quite similar, with a small difference between the iodine system and the other chlorine based systems, of 2.4\AA and 2.5\AA , respectively. Remarkably, by introducing chlorine, the methyl-ammonium dipoles near the interface seem to align in the direction of the electric field. The observed orientation of the dipoles near the interface is consistent with the orientation of the built-in electric field which is potentially enhanced in the presence of chlorine. A similar behavior was found by applying an external electric field to a MAPbI_3 slab¹⁰. Also, structural modification of the inorganic Pb-I(Cl) cages influence the rotational dynamics of dipoles^{10,34}. However, for a definitive picture of the dipole alignment at the interface molecular dynamics investigations of the interface structures are necessary.

3 Results and discussion

Recent studies suggest the chlorine plays a crucial role in the carrier transport across the interface¹⁹. Conduction band (CB) and valence band (VB) offsets as well as the charge distribution near the interface which affect the transfer effectiveness, particularly of electrons injected from the perovskite into the TiO₂ layer, are two key elements that directly influence the solar cell PCE.

We start by making an analysis based on the partial density of states (PDOS) for the structures considered in Fig. 1, where the composition of the perovskite layer is changed gradually from MAPbI₃ to MAPbCl₃. The results are presented in Fig. 2. On the left hand side of the plot the total density of states (TDOS) together with the PDOS corresponding to the MAPbI_{3-x}Cl_x perovskite and TiO₂ layers and, in addition, the sole contribution of chlorine are depicted. On the right hand side, the contributions of chlorine and iodine are indicated comparatively, for the VB of the perovskite, as their concentration ratio varies. A first observation is that the prominent Cl peak is positioned about 1-2 eV below the VB maximum, depending on the concentration, similar to the previously investigated anatase-TiO₂/MAPbI_{3-x}Cl_x structures²¹. The states associated with chlorine are displaced towards the VB maximum as the concentration of the substitutions on iodine atoms increases.

The band offsets in the vicinity of the active interface of the solar cell are essential for the charge separation. For halide perovskite solar cells, effective values have been established in the context of optimizing the carrier transport and recombination at the interface³⁵. Typically, the electrons are efficiently collected in the TiO₂ layer, while the holes are blocked at the interface. Inspecting the TDOS, one can see that all the structures present a band gap, which we will further refer to as the junction band gap. This gap appears as the two band gaps of the perovskite and TiO₂, partially overlap. They are comparable to the values for the bulk materials, in spite of the relatively small dimensions perpendicular to the interface. In particular, the VB maximum of the perovskite is found between the CB minimum and the VB maximum of the TiO₂, the results being similar to the anatase system³⁶. MAPbCl₃ is known to have a larger band gap than the iodine based counterpart and its precise distribution between the CB and VB band offsets is of importance in this context. One should note that the LDA based calculations reproduce reasonably the experimental band gap of the perovskite³⁷. Including spin-orbit coupling (SOC) in the context of local or semilocal exchange-correlation functionals, serious underestimations of the band gap are introduced³⁸⁻⁴⁰. Instead, the quasiparticle self-consistent GW approach, including the contribution from SOC³⁸, recovers the experimental band gap values found in bulk structures. However, this approach is computationally highly expensive for

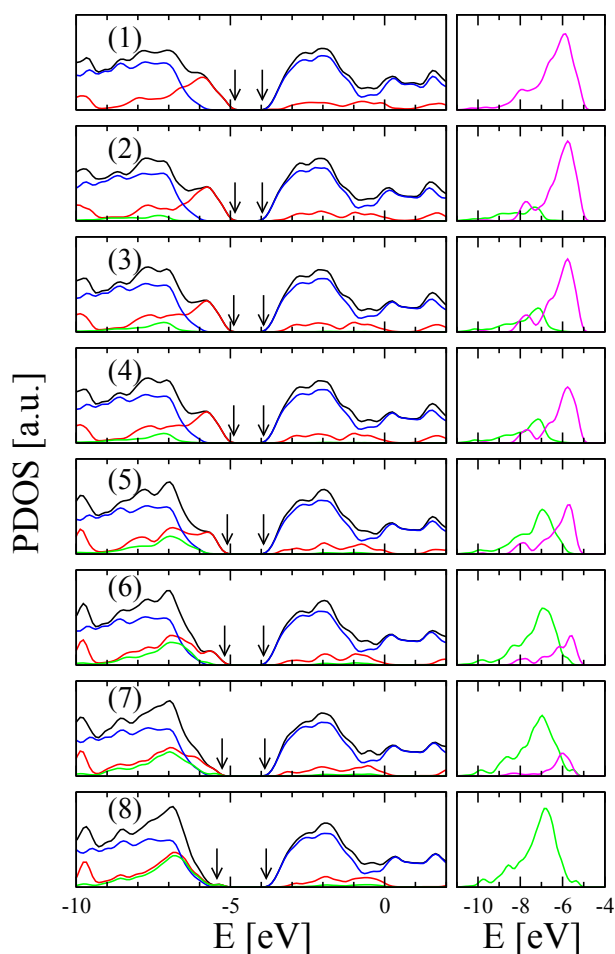


Fig. 2 Density of states analysis of the TiO₂/MAPbI_{3-x}Cl_x structures: on the left hand side, total TDOS (black) and PDOS corresponding to MAPbI_{3-x}Cl_x (red), TiO₂ (blue) and Cl (green); on the right hand side, the contributions of Cl (green) and I (magenta) to the valence band of the perovskite are indicated in detail. The junction band gap is marked by arrows. The structures (1-8) are shown in Fig. 1.

large structures²¹, as the ones considered here, being usually employed in bulk-like or smaller finite systems.

For the MAPbI₃ system, a conduction band offset of ≈ 0.6 eV is found, which is in-between the experimental⁴¹⁻⁴⁴ and the theoretical²¹ values reported for an interface based on anatase-TiO₂. As noted in the recent topical review⁴⁵ there are few studies concerning the band alignment of the TiO₂/MAPbCl₃ interface, as practical challenges restrict the usual photoelectron spectroscopy investigations. Although small variations are expected due to confinement effects in the relatively narrow slabs²¹ it should be underlined that our main results concern the comparative study of the interface systems with different compositions and subsequent modifications.

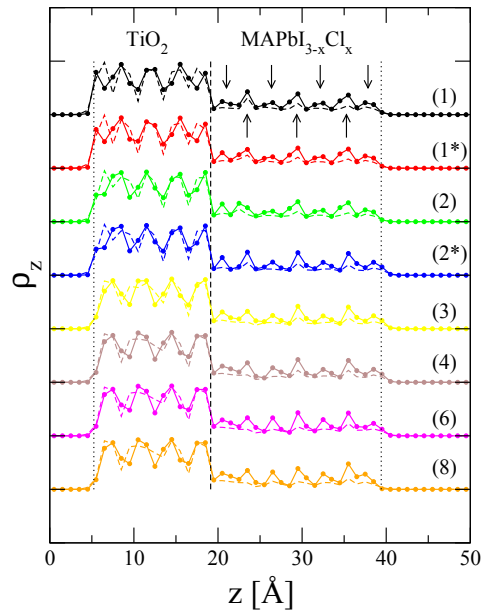


Fig. 3 Electron density (VB-solid, CB-dashed) in the slab systems along the z -direction, for the selected systems (1,2,3,4,6,8) and, additionally, the (1*) and (2*) structures described in the text. The arrows mark the the MA-I(Cl)/Pb-I(Cl) layers, respectively. The data sets are vertically shifted for better visibility. The vertical dashed line marks the interface, while the dotted lines indicate the outermost layers.

tions of CB and VB band offsets, while the values fall within the range of both experimental and theoretical investigations on similar structures. Another qualitatively similar feature is the displacement of the CB edge of TiO₂/MAPbCl₃ towards higher energy values²¹, by a comparable amount. Increasing the chlorine concentration, the CB band offset is effectively enhanced, while the VB band offset is diminished. Although the mechanism of excitonic or free carrier generation is still under debate, it is generally accepted that the carrier separation takes place at the TiO₂/MAPbI_{3-x}Cl_x. From this perspective, a larger CB band offset enhances the electron injection into the TiO₂ layer. The VB band offset is rather large for the MAPbI₃ system (≈ 1 eV) but decreases as the chlorine is added. The role of TiO₂ as hole blocking layer is therefore diminished.

Besides the band offsets, another key factor in the description of the charge transfer between the two materials is set by the charge distribution in the vicinity of the interface. Figure 3 shows the cumulative electron density, $\rho_z(z)$, defined along the z -direction as: $\rho_z(z) = \int dx \int dy \rho(x, y, z)$, where $\rho(x, y, z) = \sum_k |\Psi_k(x, y, z)|^2$ is the three-dimensional electron density, constructed from Kohn-Sham orbitals of the slab structures. In a similar way, one may consider the two-dimensional electron distributions, $\rho_{xz}(x, z) = \int dy \rho(x, y, z)$

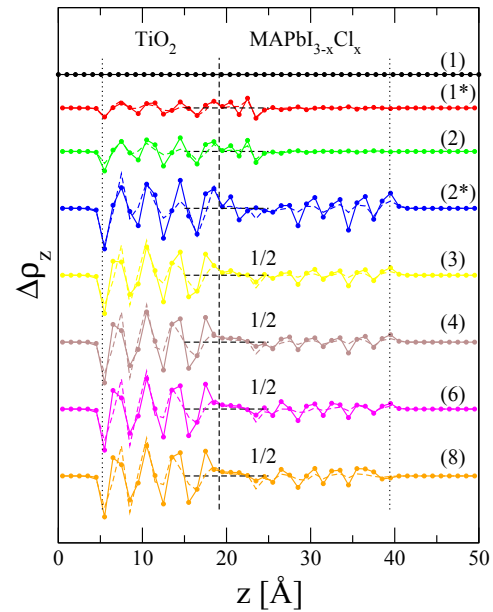


Fig. 4 Displacement of the electron density, $\Delta\rho_z(z)$, for the same structures considered in Figure 3. For a better display the values in four data sets were rescaled by 1/2.

and $\rho_{yz}(x, z) = \int dx \rho(x, y, z)$. Different energy intervals may be specified by selecting the appropriate k indices. The maxima visible for ρ_z inside the MAPbI_{3-x}Cl_x region are correlated with the MA-I(Cl) and Pb-I(Cl) layers in the perovskite slab, while similar oscillations are observed for the TiO₂ layer. For a better description we included two intermediate structures, labeled as (1*) and (2*). System (1*) has a 50% substitution of chlorine on iodine in the first Pb-I(Cl) layer. System (2*) is constructed from system (2) and an additional 50% substitution of chlorine on iodine in the first MA-I(Cl) layer. Both VB electron density and CB electron density are represented, the latter being obtained by summing up the states in a 10 eV interval above the Fermi level, showing qualitatively very similar features.

To characterize the charge transfer we introduce the displacement electron density functions, $\Delta\rho_z(z)$, $\Delta\rho_{xz}(x, z)$ and $\Delta\rho_{yz}(y, z)$, as the difference between the electron density of the systems containing chlorine and the one corresponding to the reference MAPbI₃ system (1): $\Delta\rho_z(z) = \rho_z(z) - \rho_z^{(1)}(z)$ and, in a similar way, $\Delta\rho_{xz}$ and $\Delta\rho_{yz}$. In Figure 4, $\Delta\rho_z$ is depicted for the same systems as in Fig. 3. Increasing the concentration of chlorine, oscillations develop with an enhanced magnitude in the TiO₂ layer. As we compare isoelectronic systems, the integrated charge displacement is zero. We are particularly interested in the behavior near the junction interface. Inspecting a 5-10 Å interval centered on the interface, we observe a systematic increase in the electron density, espe-

cially on the TiO_2 side. However, this increase tends to saturate rather quickly, i.e. the substitution of additional chlorine on the outer layers, e.g. the systems (5)-(8), has little effect on the interface charge distribution. This supports the idea that only the interfacial chlorine layer is actually needed to effectively change the charge transfer properties. Relative to the reference MAPbI_3 system, the extra electron charge near the interface in the chlorine based slabs is preferentially localized on the TiO_2 side, which is in line with the charge donation towards TiO_2 layer observed²¹. It is worth noting that for large enough chlorine concentration, $\Delta\rho_z(z)$ in the perovskite side drops in the negative region before it starts growing again, suggesting an electron depletion in the $\text{MAPbI}_{3-x}\text{Cl}_x$ layer near the interface. The intermediate systems (1*) and (2*) show the gradual change of the charge displacement, by increasing the chlorine substitutions. In calculating the density maps, the lower part of the TiO_2 substrate was fixed, basically ensuring the same position of the interface for the analyzed structures. Calculating the overall charge displacement in the two materials, we obtain for the structures (2), (4), (6) and (8) that 0.31, 0.34, 0.91 and 1.51% of the total charge, respectively, is transferred to the TiO_2 layer, compared with the iodine based system, showing the same trend in the charge transfer.

We extend our charge displacement analysis and plot in Fig. 5(a) two-dimensional maps for typical $\text{TiO}_2/\text{MAPbI}_{3-x}\text{Cl}_x$ interfaces. The VB electron density function $\rho_{xz}^{(1)}$ is depicted, followed by the displacement charges, $\Delta\rho_{xz}^{(i)}$, of three relevant systems, $i = 2^*, 3$ and 6 . Due to the symmetry of both perovskite and rutile- TiO_2 , the x and y directions may be interchanged with little effect on the charge densities, ρ_{xz} and ρ_{yz} , and therefore we shall only discuss in the following only one of the two functions. The system labeled as $i = 2^*$, which has less than two layers of substituted chlorine, exhibits rather small displacements, found in both materials. Increasing the chlorine concentration, the alternating sequences of positive and negative charge displacements, located mostly in the TiO_2 layer, become better defined. As already pointed out in Fig. 4, where the one-dimensional density $\Delta\rho_z$ was plotted, accumulations in the electron density on the TiO_2 side in the vicinity of the interface are visible. Concerning $\rho_{xz}^{(1)}$ one can also see in Fig. 5(a) connected pathways in the TiO_2 layer which may have a significant contribution to the electron transfer.

Using two-dimensional maps in the real space and energy, specifically the (z, E) coordinates, one obtains detailed representations of the junction band diagrams, as described in Fig. 5(b). One can comparatively see the effects introduced in the band offsets by chlorine, which are consistent with the previous PDOS analysis. The effective band gap of the perovskite increases and this results in an enhanced CB band offset and a reduced VB band offset. Decreasing the VB band offset lowers the capacity of the TiO_2 layer as the hole blocking ma-

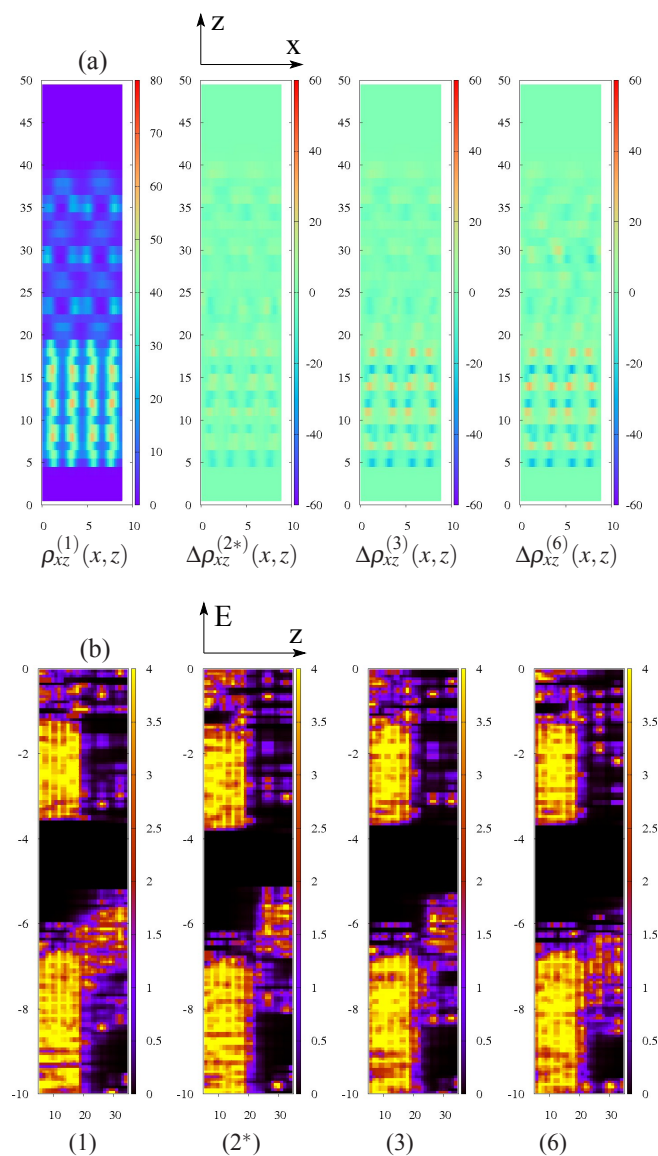


Fig. 5 (a) Electron density maps in real space (x, z) , for the MAPbI_3 system (1) and charge displacements for the (2*), (3) and (6) systems. (b) Electron density maps in (z, E) coordinates for the same structures. The units are \AA and eV, for the real space coordinates and energy, respectively. The interface is located at $z \approx 19 \text{\AA}$.

terial, while at the same time an effectively larger CB band offset may improve the electron injection from the perovskite. This suggests an optimum chlorine concentration near the interface may be found, in particular, the system (2*) showing clearly defined band offsets. In addition, the CB of the perovskite layers present a sequence of relatively narrow minibands, corresponding to the maxima in the TDOS, which are connected to a continuum of states on the TiO_2 side. In the context of electron injection from the perovskite absorber and

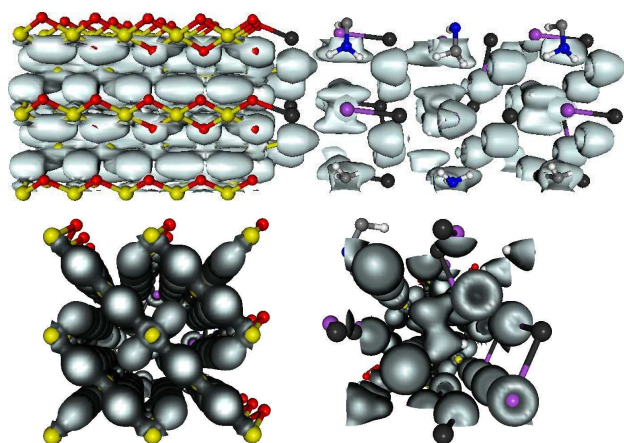


Fig. 6 Electron density $\rho^{(2)}(x,y,z)$ of structure (2): lateral and detailed views from the TiO_2 and perovskite sides.

subsequent thermalization in the TiO_2 layer, this asymmetry may reduce the probability of injected electrons to return back into the perovskite layer. Furthermore, the relatively high density of states in the CB of the TiO_2 layer may provide a substantial amount of energetically lower states which may be occupied by electrons incoming from the perovskite side. In this way the CB band offset becomes more efficient in blocking electrons stemming from the TiO_2 layer.

The picture of connected pathways in the TiO_2 layer is further confirmed by the three dimensional plot of the electron density depicted in Fig. 6 for a typical structure, where elongated overlapping orbitals are present in the TiO_2 layer. These particular chain-like shapes may favor the electron transport away from the junction, potentially reducing the interface recombination. The effects of the geometrical features of the orbitals as well as the differences in density of states in the two materials on the charge transfer should be further explored.

4 Conclusions

Rutile- $\text{TiO}_2/\text{MAPbI}_{3-x}\text{Cl}_x$ interfaces were investigated by *initio* DFT calculations, with the focus on the role played by the chlorine in the band alignment and the charge distribution across the interface, which directly impacts the solar cell efficiency. We found similar generic features in the rutile systems, as in the case of the previously analyzed anatase- TiO_2 structures, regarding the band alignment in iodine based systems and the contribution of chlorine to the density of states of the junction systems. In addition, performing a systematic analysis for different chlorine concentrations, the optimum conditions for the charge separation are discussed.

First, the changes in the conduction and valence band offsets are investigated. Introducing chlorine substitutions on io-

dine, the perovskite band gap increases, leading to an enhancement of the conduction band offset. This should improve the electron injection into the TiO_2 layer. At the same time, the valence band offset decreases, which becomes detrimental for hole separation, suggesting that only limited interfacial chlorine substitution is optimal.

Furthermore, the charge transfer was investigated using a displacement charge technique. Compared to the structure based on the MAPbI_3 perovskite, the chlorine systems show an extra amount of electron charge localized in the TiO_2 layer in the vicinity of the interface. It was also established that the charge transfer tends to saturate with the chlorine concentration.

As discussed in the end of the previous section, the specific asymmetries in the band structure at both sides of the interface may also aid the electron transfer. Taking into account both the changes induced in the band alignment and charge transfer, one may suggest that adjusting the chlorine concentration near the $\text{TiO}_2/\text{MAPbI}_{3-x}\text{Cl}_x$ interface may provide an important path in optimizing the solar cells efficiency.

Acknowledgements

The research leading to these results has received funding from EEA Financial Mechanism 2009 - 2014 under the project contract no 8SEE/30.06.2014. We are thankful to Ioana and Lucian Pintilie for instructive discussions.

References

- 1 A. Kojima, K. Teshima, Y. Shirai and T. Miyasaka, *J. Am. Chem. Soc.*, 2009, **131**, 6050.
- 2 N. G. Park, *J. Phys. Chem. Lett.*, 2013, **4**, 2423.
- 3 N. J. Jeon, J. H. Noh, W. S. Yang, Y. C. Kim, S. Ryu, J. Seo and S. I. Seok, *Nature*, 2015, **517**, 476.
- 4 G. Xing, N. Mathews, S. Sun, S. S. Lim, Y. M. Lam, M. Grätzel, S. Mhaisalkar and T. C. Sum, *Science*, 2013, **342**, 344.
- 5 J. M. Frost, K. T. Butler, F. Brivio, C. H. Hendon, M. van Schilfhaarde and A. Walsh, *Nano Lett.*, 2014, **14**, 2584.
- 6 J. M. Frost, K. T. Butler and A. Walsh, *APL Mater.*, 2014, **2**, 081506.
- 7 E. Mosconi, C. Quarti, T. Ivanovska, G. Ruani and F. D. Angelis, *Phys. Chem. Chem. Phys.*, 2014, **16**, 16137.
- 8 J. Ma and L.-W. Wang, *Nano Lett.*, 2015, **15**, 248.
- 9 A. Mattoni, A. Filippetti, M. I. Saba and P. Delugas, *J. Phys. Chem. C*, 2015, **119**, 17421.
- 10 C. Goehry, G. A. Nemnes and A. Manolescu, *J. Phys. Chem. C*, 2015, **119**, 19674.
- 11 G. Niu, X. Guoa and L. Wang, *J. Mater. Chem. A*, 2015, **3**, 8970.
- 12 S. Colella, E. Mosconi, P. Fedeli, A. Listorti, F. Gazza, F. Orlandi, P. Ferro, T. Besagni, A. Rizzo, G. Calestani, G. Gigli, F. D. Angelis and R. Mosca, *Chem. Mater.*, 2013, **23**, 4613.
- 13 B. Suarez, V. Gonzalez-Pedro, T. S. Ripolles, R. S. Sanchez, L. Otero and I. Mora-Sero, *J. Phys. Chem. Lett.*, 2014, **5**, 1628.
- 14 S. D. Stranks, G. E. Eperon, G. Grancini, C. Menelaou, M. J. P. Alcocer, T. Leijtens, L. M. Herz, A. Petrozza and H. Snaith, *Science*, 2013, **342**, 341.

- 15 C. Wehrenfennig, G. E. Eperon, M. B. Johnston, H. J. Snaith and L. M. Herz, *Adv. Mater.*, 2014, **26**, 1584.
- 16 S. T. Williams, F. Zuo, C.-C. Chueh, C.-Y. Liao, P.-W. Liang and A. K.-Y. Jen, *ACS Nano*, 2014, **8**, 10640.
- 17 H. Yu, F. Wang, F. Xie, W. Li1, J. Chen and N. Zhao, *Adv. Funct. Mater.*, 2014, **24**, 7102.
- 18 E. Edri, S. Kirmayer, M. Kulbak, G. Hodes and D. Cahen, *J. Phys. Chem. Lett.*, 2014, **5**, 429.
- 19 Q. Chen, H. Zhou and Y. F. et al., *Nature Commun.*, 2015, **6**, 7269.
- 20 D. E. Starr, G. Sadoughi, E. Handick, R. G. Wilks, J. H. Alsmeier, L. Köhler, M. Gorgoi, H. J. Snaith and M. Bär, *Energy Environ. Sci.*, 2015, **8**, 1609.
- 21 E. Mosconi, E. Ronca and F. D. Angelis, *J. Phys. Phys. Chem. Lett.*, 2014, **5**, 2619.
- 22 S. Colella, E. Mosconi, G. Pellegrino, A. Alberti, V. L. P. Guerra, S. Masi, A. Listorti, A. Rizzo, G. G. Condorelli, F. D. Angelis and G. Gigli, *J. Phys. Chem. Lett.*, 2014, **5**, 3532.
- 23 H. S. Kim, J. W. Lee, N. Yantara, P. P. Boix, S. A. Kulkarni, S. Mhaisalkar, M. Grätzel and N. G. Park, *Nano Lett.*, 2013, **13**, 2412.
- 24 Q. Jiang, X. Sheng, Y. Li, X. Feng and T. Xu, *Chem. Commun.*, 2014, **50**, 14720.
- 25 J.-W. Lee, T.-Y. Lee, P. J. Yoo, M. Grätzel, S. Mhaisalkard and N.-G. Park, *J. Mater. Chem. A*, 2014, **2**, 9251.
- 26 A. Yella, L. P. Heiniger, P. Gao, M. K. Nazeeruddin and M. Grätzel, *Nano Lett.*, 2014, **14**, 2591.
- 27 A. Fakhruddin, F. D. Giacomo, I. Ahmed, Q. Wali, T. M. Brown and R. Jose, *J. Power Sources*, 2015, **283**, 61.
- 28 B. Cai, D. Zhong, Z. Yang, B. Huang, S. Miao, W.-H. Zhang, J. Qiu and C. Lib, *J. Mater. Chem. C*, 2015, **3**, 729.
- 29 J.-F. Li, Z.-L. Zhang, H.-P. Gao, Y. Zhanga and Y.-L. Mao, *J. Mater. Chem. A*, 2015, DOI:10.1039/C5TA03765D.
- 30 G. S. Han, H. S. Chung, D. H. Kim, B. J. Kim, J.-W. Lee, N.-G. Park, I. S. Cho, J.-K. Lee, S. Lee and H. S. Jung, *Nanoscale*, 2015, DOI:10.1039/C5NR03476K.
- 31 J. Soler, E. Artacho, J. D. Gale, A. Garcia, J. Junquera, P. Ordejon and D. Sanchez-Portal, *J. Phys. Condens. Matter.*, 2002, **14**, 2745.
- 32 D. M. Ceperley and B. J. Alder, *Method. Phys. Rev. Lett.*, 1980, **45**, 566.
- 33 K. T. Butler, J. M. Frost and A. Walsh, *Mater. Horiz.*, 2015, **2**, 228.
- 34 E. Mosconi, C. Quarti, T. Ivanovska, G. Ruani and F. D. Angelis, *Phys. Chem. Chem. Phys.*, 2014, **16**, 16137.
- 35 T. Minemoto and M. Murata, *Solar Energy Materials and Solar Cells*, 2015, **133**, 814.
- 36 F. D. Angelis, *Acc. Chem. Res.*, 2014, **47**, 3349.
- 37 Y. Yamada, T. Nakamura, M. Endo, A. Wakamiya and Y. Kanemitsu, *Appl. Phys. Express*, 2014, **7**, 032302.
- 38 F. Brivio, K. T. Butler and A. Walsh, *Phys. Rev. B*, 2014, **89**, 155204.
- 39 J. Even, L. Pedesseau, J.-M. Jancu and C. Katan, *J. Phys. Chem. Lett.*, 2013, **4**, 2999.
- 40 G. Giorgi, J.-I. Fujisawa, H. Segawa and K. Yamashita, *J. Phys. Chem. Lett.*, 2013, **4**, 4213.
- 41 H.-S. Kim, C.-R. Lee, J.-H. Im, K.-B. Lee, T. Moehl, A. Marchioro, S.-J. Moon, R. Humphry-Baker, J.-H. Yum, J. E. Moser, M. Grätzel and N.-G. Park, *Sci. Rep.*, 2012, **2**, 591.
- 42 W. Ke, G. Fang, J. Wang, P. Qin, H. Tao, H. Lei, Q. Liu, X. Dai and X. Zhao, *Appl. Mater. Interfaces*, 2014, **6**, 15959.
- 43 R. Lindblad, D. Bi, B. w. Park, J. Oscarsson, M. Gorgoi, H. Siegbahn, M. Odellius, E. M. J. Johansson and H. Rensmo, *Phys. Chem. Lett.*, 2014, **5**, 648.
- 44 P. Cottingham, D. C. Wallace, K. Hu, G. Meyer and T. M. McQueen, *Chem. Commun.*, 2015, **51**, 7309.
- 45 T. C. Sum, S. Chen, G. Xing, X. Liu and B. Wu, *Nanotechnology*, 2015, **26**, 342001.